

Predicting Frictional Properties of Graphene Kirigami Using Molecular Dynamics and Neural Networks

Designs for a negative friction coefficient.

Mikkel Metzsch Jensen



Thesis submitted for the degree of
Master in Computational Science: Materials Science
60 credits

Department of Physics
Faculty of mathematics and natural sciences

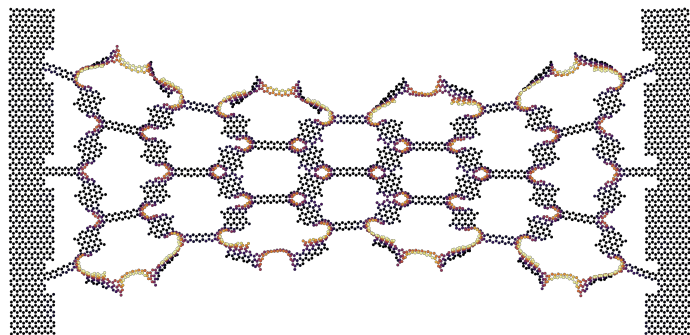
UNIVERSITY OF OSLO

Spring 2023

Predicting Frictional Properties of Graphene Kirigami Using Molecular Dynamics and Neural Networks

Designs for a negative friction coefficient.

Mikkel Metzsch Jensen



© 2023 Mikkel Metzsch Jensen

Predicting Frictional Properties of Graphene Kirigami Using Molecular Dynamics and Neural Networks

<http://www.duo.uio.no/>

Printed: Reprocentralen, University of Oslo

Abstract

Abstract.

Acknowledgments

Acknowledgments.

List of Symbols

F_N Normal force (normal load)

Acronyms

AFM Atomic Force microscope. 17, 18, 19, 20, 21

FFM Friction Force Microscopes. 17, 18, 19, 20

FK Frenkel-Kontorova. 7, 12, 13, 14, 15, 16, 19, 20

FKT Frenkel–Kontorova–Tomlinson. 7, 16, 19, 20

GS Ground State. 13, 14

MD Molecular Dynamics. 6, 7, 8, 10, 19, 20, 21, 22

PT Prandtl–Tomlinson. 7, 12, 13, 15, 16, 18, 19, 20, 21

SFA Surface force apparatus. 18, 19

SFM Scanning Force Microscopies. 17

SPM Scanning Probe Microscopy. 17

Contents

I Background Theory	1
1 Friction	3
1.1 Friction across scales	3
1.2 Macroscale	3
1.2.1 Amontons' law	4
1.3 Microscopic scale	5
1.3.1 Asperity theories	5
1.4 Nanoscale — Atomic scale	6
1.4.1 Prandtl–Tomlinson	7
1.4.1.1 Thermal activation	8
1.4.1.2 Sliding speed	10
1.4.1.3 Tip mass	11
1.4.1.4 Friction Regimes: Smooth Sliding, Single Slip, and Multiple Slip	11
1.4.2 Frenkel-Kontorova	12
1.4.2.1 Commensurability	13
1.4.2.2 Velocity resonance	15
1.4.3 Frenkel-Kontorova-Tomlinson	16
1.4.4 Shortcomings of atomic models	17
1.4.5 Experimental procedures	17
1.4.5.1 Scanning Probe Microscopy	17
1.4.5.2 Surface Force Apparatus	18
1.5 Summary of previous results	18
1.6 Research questions	22
II Simulations	23
Appendices	25
Appendix A	27
Appendix B	29
Appendix C	31

Part I

Background Theory

Chapter 1

Friction

Since we aim for controlling frictional properties, we will review the relevant theoretical understanding of friction in this chapter. We will relate the theory to our study and highlight some of the expected outcomes. In this thesis, we will only concern ourselves with dry friction, i.e. without any use of lubrication, and without any resulting wear of the contacting surfaces.

1.1 Friction across scales

Tribological systems span a wide range of time and length scales, from geological stratum layers involved in earthquakes [1] to atomistic processes, such as the gliding motion of nanoclusters or nanomotors [2]. This vast difference in scale leads to different dominant frictional mechanisms. At the macro scale, systems are typically subject to relatively high loads and sliding speeds, resulting in significant contact stress and wear. On the other hand, the micro-/nanoscale regime occupies the opposite domain operating under a relatively small load and sliding speed with negligible wear [1] [3, p. 5]. While macroscale friction is often reduced into a few variables such as load, material type, sliding speed and surface roughness, it is clear that the micro-/nanoscale friction cannot be generalized under such a simple representation. On the micro-/nanoscale the tribological properties are dominated by surface properties which will yield a more complex behavior of said variables and introduce an additional sensitivity to variables such as temperature, humidity and even sliding history. The works of Bhushan and Kulkarni [4] showed that the friction coefficient decreased with scale even though the materials used were unchanged. This reveals an intrinsic relationship between friction and scale as the contact condition is altered.

The phenomenological descriptions of macroscale friction cannot yet be derived from the fundamental atomic principles, and bridging the gap between different length scales in tribological systems remains an open challenge [2]. Hence, the following sections will be organized into macroscale (Sec. 1.2), microscale (Sec. 1.3) and nanoscale (Sec. 1.4) representing the theoretical understanding governing each scale regime. Realizing that the field of tribology across all scales is a vastly broad and intricate topic, we will aim to introduce only the essential findings for each scale, while keeping a main focus on necessary theoretical background associated with the understanding of our system of interest which takes place at the nanoscale.

1.2 Macroscale

Our working definition of the *macroscale* is everything on the scale of visible objects. This is usually denoted to the size of millimeters 10^{-3} m and above. Most importantly, we want to make a distinction to the microscale, where the prefix indicates the size of micrometers m^{-6} . Hence, we essentially consider everything larger than *micro* to belong to the macroscale¹.

¹The width of a human hair is often used as a reference for the limit of human perception. Since the width of a human hair is on the length scale 10^{-5} to 10^{-4} m we find this limit aligns rather well with the defined transition from macro- to microscale.

1.2.1 Amontons' law

In order to start and keep a solid block moving against a solid surface we must overcome certain frictional forces F_{fric} [5]. The static friction force F_s corresponds to the minimum tangential force required to initiate the sliding while the kinetic friction force F_k corresponds to the tangential force needed to sustain such a sliding at a steady speed. The work of Leonardo da Vinci (1452–1519), Guillaume Amontons (1663–705) and Charles de Coulomb (1736–1806) all contributed to the empirical law, commonly known as *Amontons' law*, which serves as a common base for macroscale friction. Amontons' law states that the frictional forces are entirely independent of contact area and sliding velocity. Instead, it relies only on the normal force F_N , acting perpendicular to the surface, and the material-specific friction coefficient μ as

$$F_{\text{fric}} = \mu F_N. \quad (1.1)$$

Notice that the term *normal force* is often used interchangeably with *load* and *normal load* although the load and normal load refer to the applied force that pushes the object into the surface, whereas the normal force is the reaction force acting from the surface on the object. In equilibrium, these forces are equal in magnitude and opposite in direction, and hence we will not make a distinction between these terms. On the same note, we point out that the frictional force is different from a conventional force which in the Newtonian definition acts on a body from the outside and makes it accelerate [6]. Rather than being an independent external force the friction force is an internal *reaction* force opposing the externally applied “sliding” force.

The friction coefficient μ is typically different for the cases of static (μ_s) and kinetic (μ_k) friction, usually both with values lower than one and $\mu_s \geq \mu_k$ in all cases [5, p. 6]. The friction coefficient is taken to be a constant defined by either [6]

$$\mu_1 = \frac{F_{\text{fric}}}{F_N}, \quad (1.2a) \quad \text{or} \quad \mu_2 = \frac{dF_{\text{fric}}}{dF_N}. \quad (1.2b)$$

The first definition Eq. (1.2a) requires zero friction at zero load, i.e. $F_{\text{fric}} = 0$ at $F_N = 0$, while the second definition Eq. (1.2b) allows for a finite friction force at zero load as the coefficient is defined by the slope of the $F_{\text{fric}}-F_N$ -curve. The consequences of these definitions are illustrated in Fig. 1.1, for selected $F_{\text{fric}}-F_N$ -curves in Fig. 1.1a and corresponding friction coefficients in Fig. 1.1b and Fig. 1.1c. For adhesive contacts, the friction force will not be zero under zero load (red curve: Linear + shift) which can be mitigated by adding an extra constant to Eq. (1.1) [6]. Using Eq. (1.2a) for adhesive contacts would make the friction coefficient diverge for decreasing load as illustrated in Fig. 1.1b. Thus, we find the second definition Eq. (1.2b) more robust and versatile. This also allows for a better interpretation of the friction coefficient in the case where friction depends non-linearly on load (Purple curve in Fig. 1.1).

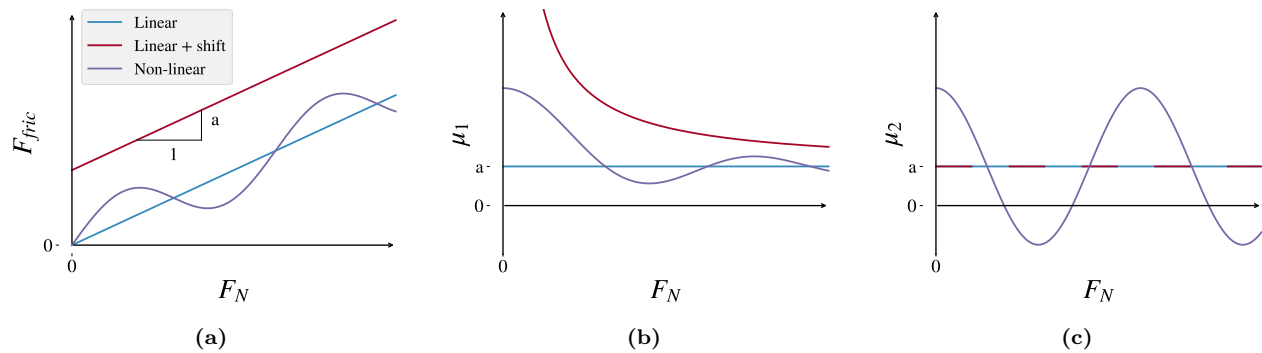


Figure 1.1: CAPTION

Amontons' law represents the behavior relatively accurately for many surfaces in contact, involving both dry and lubricated, ductile and brittle and rough and smooth surfaces (as long as they are not adhesive) under a variety of conditions [6]. But it has its limitations. For instance, at low velocities, Amontons' model breaks down due to thermal effects, and for high velocities due to inertial effects [5, pp. 5–6]. Additionally, static friction depends on the so-called contact history, with increasing static friction as the logarithm of time in stationary contact [7].

In cases where Amontons' law breaks down, we might still use the conceptual definition of the friction coefficient as defined by (Eq. (1.2b)). Especially, in the context of achieving negative friction coefficients (in certain load ranges), we would refer to this definition, since Eq. (1.2a) would imply a truly unphysical situation of the frictional force acting in the same direction as the sliding motion. This would accelerate the object indefinitely².

Due to the empirical foundation of Amontons' law, it does not provide any physical insight into the underlying mechanisms of friction. However, as we will later discuss in more detail, we can understand the overall phenomena of friction through statistical mechanics by the concept of *equipartition of energy* [2]. A system in equilibrium has its kinetic energy uniformly distributed among all its degrees of freedom. When a macroscale object is sliding in a given direction it is clearly not in equilibrium since one of its degrees of freedom carries considerably more kinetic energy. Thus, the system will have a tendency to transfer kinetic energy to the remaining degrees of freedom in the form of heat dissipating to the surroundings and making the object slow down if not continuously driven forward by an external energy source. Hence, we can understand the overall concept of friction simply as the tendency of going toward equilibrium energy equipartitioning among many interacting degrees of freedom [2]. From this point of view, it is clear that friction is an inevitable part of contact physics, but even though friction cannot be removed altogether, we are still capable of manipulating it in useful ways.

The attentive reader might point out that we have already moved the discussion into the microscopic regime as *statistical mechanics* generally aim to explain macroscale behavior by microscopic interactions. In fact, this highlights the necessity to consider smaller scales in order to achieve a more fundamental understanding of friction.

Mot slutten av 2.2 kan du kommentere at det finnes mer avanserte makroskopiske modeller, men at Amontons lov gir oss det konseptuelle som vi trenger i akkurat denne studien.

1.3 Microscopic scale

Going from a macro- to a microscale perspective, at a length scale on the order 10^{-6} m, it was realised that most surfaces are in fact rough [8]. The contact between two surfaces consists of numerous smaller contact points, so-called *asperities*, which form junctions due to contact pressure and adhesion as visualized in Fig. 1.2 [1]. In the macroscale perspective of Amonton's law, we refer to time- and space-averaged values, i.e. the apparent contact area and the average sliding speed [6]. However, microscopically we find the real contact area to be much smaller than the apparent area [1], and the shearing motion of local microjunctions to happen at large fluctuations rather than as one synchronized movement throughout the surface.

It is generally accepted that friction is caused by two mechanisms: Mechanical friction and chemical friction [1]. Mechanical friction is the “plowing” of the surface by hard particles or said asperities with an energy loss attributed to deformations of the asperity. While plastic deformations, corresponding to wear, gives rise to an obvious attribution for the energy loss, elastic deformations are also sufficient in explaining energy loss due to phonon excitations. The assumption of plastic deformations has been criticized as this is theorized only to be present at the beginning of a surface contact while it is negligible for prolonged or repeated contacts [9]. That is, when machine parts slide against each other for millions of cycles, the plastic deformation would only take place at the beginning for which the system then reaches a steady state with only elastic deformations. The chemical friction arises from adhesion between microscopic contacting surfaces, with an energy loss attributed to the breaking and forming of bonds. What kind of bonds

1.3.1 Asperity theories

Asperity theories have their foundations in the adhesion model proposed by Bowden and Tabor [10] which is based on the fundamental reasoning that friction is governed by the adhesion between two surfaces [11]. Adhesion is proportional to the real contact area defined by asperity junctions and interfacial shear strength τ between such contacting junctions. For an asperity contact area A_{asp} we get a true contact area $\sum A_{\text{asp}}$ leading to

$$F_{\text{fric}} = \tau \sum A_{\text{asp}}.$$

²You would most likely have a good shot at the Nobel Prize with that paper.

Note that this is still compatible with Amontons' law in Eq. (1.1) by having a linear relationship between the real contact area and the applied load. In fact, this is exactly how the theoretical model explains the friction dependency of load. By increasing the normal load it is hypothesized that the real contact area will increase as the asperity tips are deformed (plastically or elastically) into broader contact points as visualized qualitatively in Fig. 1.2.

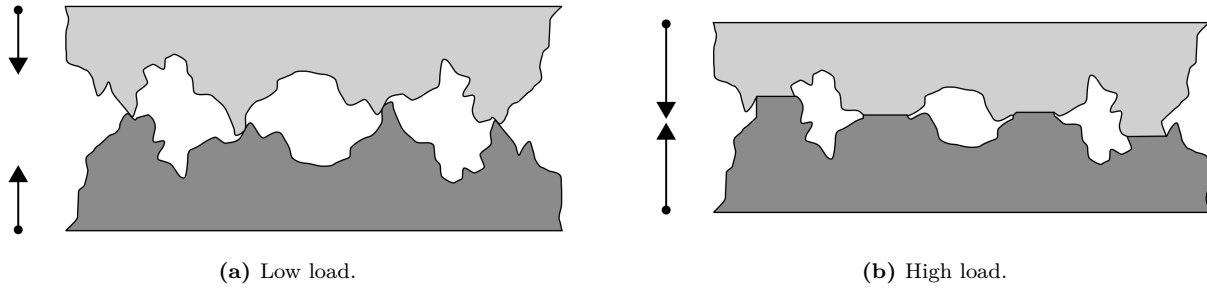


Figure 1.2: Qualitative illustration of the microscopic asperity deformation under increasing load from frame (a) to (b) [12]. While this figure seemingly portrays plastic deformation the concept of increased contact area under increased load applies to elastic deformation as well.

Many studies have focused on single asperity contacts to reveal the relationship between the contact area and load [13–15]. By assuming perfectly smooth asperities, with radii of curvature from micrometers all the way down to nanometers, continuum mechanics can be used to predict the deformation of asperities as load is applied. A model for non-adhesive contact between homogenous, isotropic, linear elastic spheres was first developed by Hertz [16], which predicted $A_{\text{asp}} \propto F_N^{2/3}$. Later adhesion effects were included in a number of subsequent models, including Maugis-Dugdale theory [17], which also predicts a sublinear relationship between A_{asp} and F_N . Thus, the common feature of all single-asperity theories is that A_{asp} is a sublinear function of F_N , leading to a similar sublinear relationship for $F_{\text{fric}}(F_N)$, which fails to align with the macroscale observations modeled by Amontons' law (eq. (1.1)).

Concurrently with single-asperity studies, roughness contact theories are being developed [18–21] to bridge the gap between single asperities and macroscopic contacts [8]. A variety of multi-asperity theories has attempted to combine single asperity mechanics by statistical modeling of the asperity height and spatial distributions [9]. This has led to partial success in the establishment of a linear relationship between A_{asp} and F_N . Unfortunately, these results are restricted in terms of the magnitude of the load and contact area, where multi-asperity contact models based on the original ideas of Greenwood and Williamson [20] only predicts linearity at vanishing low loads, or Persson [19] which predicts linearity for more reasonable loads but only up to 10–15 % of the macroscale contact area. However, as the load is further increased all multi-asperity models predict the contact area to fall into the sublinear dependency of normal force as seen for single asperity theories as well [9].

1.4 Nanoscale — Atomic scale

Going from a micro- to a nanoscale, on the order of 10^{-9} m, it has been predicted that continuum mechanics will start to break down [22] due to the discreteness of individual atoms. In a numerical MD study by Mo et al. [8], considering asperity radii of 5–30 nm, it has been shown that the asperity area A_{asp} , defined by the circumference of the contact zone, is sublinear with F_N . This is accommodated by the observation that not all atoms within the circumference make chemical contact with the substrate. By modeling the real contact area $A_{\text{real}} = N A_{\text{atom}}$, where N is the amount of atoms within the range of chemical interaction and A_{atom} the associated surface area for a contacting atom, they found a consistent linear relationship between friction and the real contact area. Without adhesive forces this leads to a similar linear relationship $F_{\text{fric}} \propto F_N$, while adding van der Waals adhesion to the simulation gave a sublinear relationship matching microscale single asperity theory, even though the $F_{\text{fric}} \propto A_{\text{real}}$ was maintained. This result emphasizes that the predictions of continuum mechanics might still apply at the nanoscale and that the contact area can still be expected to play an important role for nanoscale asperity contact. It is simply the definition of the contact area that undergoes a change when transitioning from micro- to nanoscale.

While the study by Mo et al. [8] considers a single asperity on a nanoscale, some models take this even further to what we will denote as the atomic-scale. This final leap is motivated by the fact that our system of interest, an atomically flat graphene sheet imposed on a flat silicon substrate, lacks the presence of nanoscale asperities in its initial uncut undeformed state. In the lack of noteworthy structural asperities, friction can instead be modeled as a consequence of the “rough” potential laid out by the atomic landscape. A series of so-called reduced-order models build on a simplified system of atomic-scale contacts based on three essential parts: 1) A periodic potential modeling the substrate as a rigid crystalline surface. 2) An interacting particle, or collection of particles, placed in the potential. 3) A moving body, moving at a steady speed, and connected to the particles through a harmonic coupling. In figure Fig. 1.3 three of the most common 1D models are displayed which we will address in the following sections. The time-honored Prandtl-Tomlinson (PT) model describes a point-like tip sliding over a space-periodic fixed crystalline surface with a harmonic coupling to the moving body. This is analog to that of an experimental cantilever used for Atomic Force Microscopy which we will introduce in more detail in Sec. 1.4.5.1. Further extensions were added in the Frenkel-Kontorova (FK) model by substituting the tip with a chain of harmonically coupled particles dragged from the end, and finally combined in the Frenkel-Kontorova-Tomlinson (FKT) with the addition of a more rigorous harmonic coupling between the moving body and each of the atoms in the chain. While these models cannot provide the same level of detail as atomistic simulations such as MD they enable investigation of atomic friction under most conditions, some of which are inaccessible to MD [23]. This makes these models an appropriate tool for investigating individual parameters and mechanisms governing affecting friction.

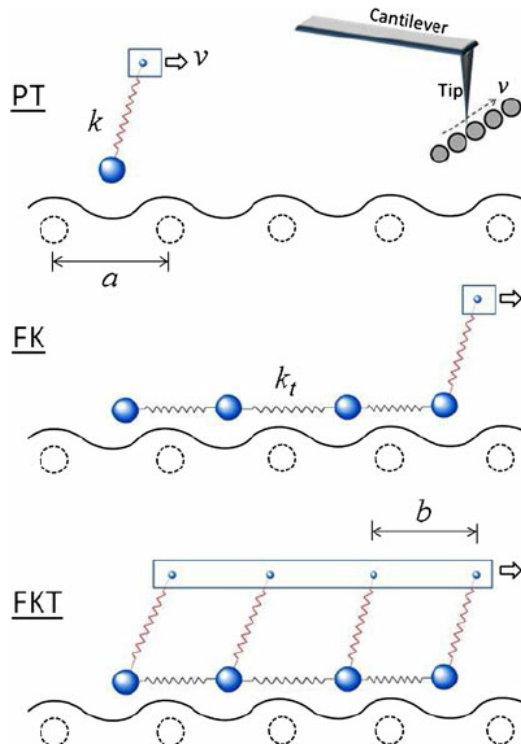


Figure 1.3: Temporary figure from [23]. Be careful to align the notation on the figures with the text later on.

1.4.1 Prandtl–Tomlinson

We consider the Prandtl–Tomlinson model (PT) with added thermal activation as proposed by Gnecco et al. [24]. For the theoretical foundation of this section, we generally refer to [23].

The 1D PT model assumes a single ball-tip coupled harmonically to a support moving at a constant speed which makes the tip slide along the rigid substrate. The interaction between tip and substrate is modeled as a sinusoidal corrugation potential mimicking the periodicity found in a crystalline substrate. The total potential

energy is given as

$$V(x, t) = \frac{1}{2}K(vt - x)^2 - \frac{1}{2}U_0 \cos\left(\frac{2\pi x}{a}\right). \quad (1.3)$$

The first term describes the harmonic coupling at time t , with spring constant K , between the tip at position x and the moving body at position vt , given by its constant speed v . The second term describes the corrugation potential with amplitude U_0 and period a representing the lattice spacing of the substrate. The dynamics of the tip can be described by the Langevin equations

$$m\ddot{x} + m\mu\dot{x} = -\frac{\partial V(x, t)}{\partial x} + \xi(t), \quad (1.4)$$

Match notation with later use.

where m is the mass of the tip, μ the viscous friction and $\xi(t)$ the thermal activation term. The equation is solved for tip position x and the friction force is retrieved as the force acting on the moving body

$$F_{\text{fric}} = K(vt - x).$$

The governing equation Eq. (1.4) belongs to a family of stochastic differential equations composed of deterministic dynamics and stochastic processes. In this case, the deterministic term is the viscous friction, $m\mu\dot{x}$, to resist the movement of the tip and the force acting from the corrugation potential. The stochastic term is a random force field modeling thermal noise according to the fluctuation–dissipation relation. Thus, there is no single path but rather multiple paths the tip can take. While the Langevin equations is one of the most common ways to handle thermal activation other methods exist to solve this problem such as Monte Carlo sampling methods. We omit the numerical scheme for solving this and refer to a more in-depth discussion of the Langevin equations with respect to the use in MD simulations in ??.

1.4.1.1 Thermal activation

The solving of the Langevin equations, as opposed to Newton's equation of motion, introduces thermal effects to the system. Generally, when the energy barrier comes close to $k_B T$ (0.026 eV at room temperature) thermal effects can not be neglected. In the case of a single asperity contact the energy barrier is on the order 1 eV which makes thermal activation significant [23]. Due to the moving body traveling at a constant speed, the potential energy will increase steadily. Without any temperature, $T = 0$, the slip will only occur when the energy barrier between the current potential well (i) and the adjacent (j) is zero $\Delta V_{i \rightarrow j} = 0$. However, in the presence of temperature, we get thermal activation, meaning that the tip can slip to the next potential well sooner $\Delta V_{i \rightarrow j} > 0$. Provided that the sliding speed is slow enough (Elaborate) the transition rate κ for a slip from the current to the next well is given by

$$\kappa = f_0 e^{-\Delta V/k_B T}, \quad (1.5)$$

with ΔV being the energy barrier and f_0 the attempt rate. The attempt rate following Kramer's rate theory [25] is related to the mass and damping of the system and can be thought of as the frequency at which the tip “attempts” to overcome the barrier. Notice that Eq. (1.5) resembles a microstate probability in the canonical ensemble with f_0 in place of the inverse partition function Z^{-1} which can be used as another interpretation of f_0 . The probability p_i that the tip occupies the current well i relative to the adjacent well j , as illustrated in Fig. 1.4 is governed by

$$\frac{dp_i}{dt} = -\kappa_{i \rightarrow j} p_i + \kappa_{j \rightarrow i} p_j.$$

This probability is related to temperature, speed and mass.

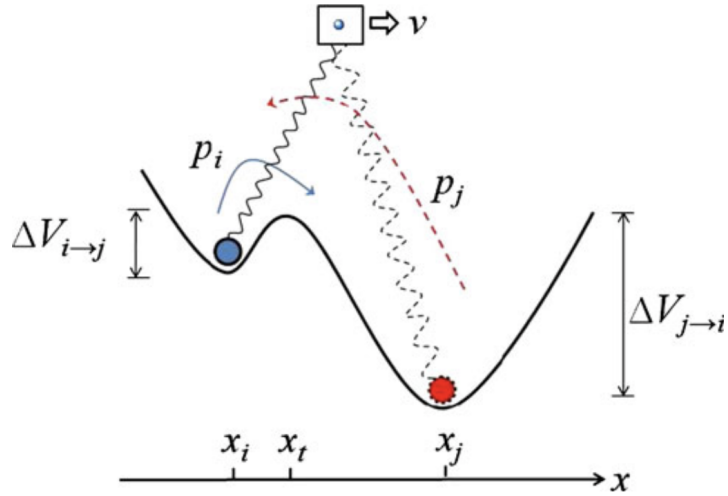


Fig. 3 An illustration of slip between two adjacent energy minima. p_i is the probability of the tip residing in the current potential well, i , where the energy barrier is $\Delta V_{i \rightarrow j}$. p_j is the probability of the tip residing at the next minima, j , where $\Delta V_{j \rightarrow i}$ is the corresponding energy barrier

Figure 1.4: [Temporary] figure from [23]

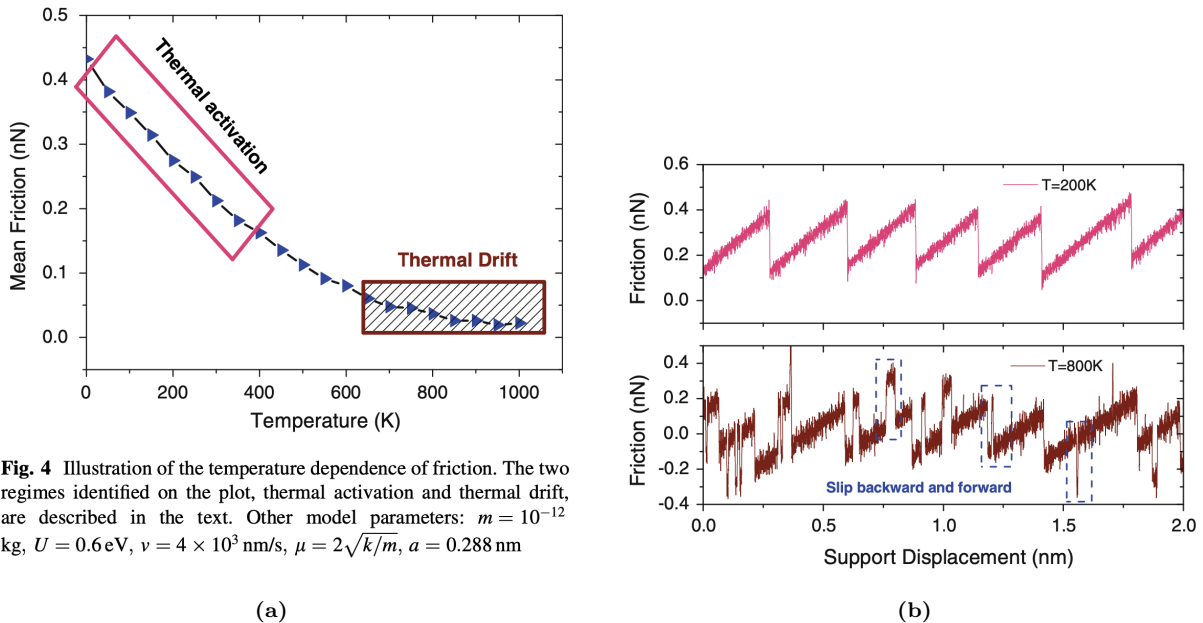


Fig. 4 Illustration of the temperature dependence of friction. The two regimes identified on the plot, thermal activation and thermal drift, are described in the text. Other model parameters: $m = 10^{-12}$ kg, $U = 0.6$ eV, $v = 4 \times 10^3$ nm/s, $\mu = 2\sqrt{k/m}$, $a = 0.288$ nm

Figure 1.5: [Temporary] figures from [23]

Generally, there exist two temperature regimes in the model: Thermal activation at low temperatures and thermal drift at high temperatures as shown in Fig. 1.5. At lower temperatures, the system is subject to standard thermal activation with $\Delta V_{i \rightarrow j} \gg \Delta V_{j \rightarrow i}$ resulting in $\kappa V_{i \rightarrow j} \gg \kappa V_{j \rightarrow i}$. Effectively, this inhibits any backward

slip and we get

$$\frac{dp_i}{dt} = -\kappa_{i \rightarrow j} p_i,$$

which makes the relationship between friction, temperature and speed follow Sang et al.'s prediction [26]

$$F = F_c - \left| \beta k_B T \ln \left(\frac{v_c}{v} \right) \right|^{2/3}, \quad v_c = \frac{2f_0 \beta k_B T}{3C_{\text{eff}} \sqrt{F_c}}, \quad (1.6)$$

where F_c is the maximum friction at $T = 0$, v_c a critical velocity, f_0 is the attempt rate, C_{eff} the effective stiffness, and β a parameter determined by the shape of the corrugation well. Eq. (1.6) characterizes the decrease in friction with temperature in the thermal activation regime, shown in Fig. 1.5a at low temperature, with the assumption of only forward slips, as seen in the force trace shown in Fig. 1.5a. When the temperature is high enough, for the system to be consistently close to thermal equilibrium, it enters the regime of thermal drift [27]. This regime transition can be understood through a comparison of two time scales: The time it takes for the moving body to travel one lattice spacing $t_v = a/v$ and the average time for a slip to occur due to thermal activation $\tau = 1/\kappa = f^{-1} \exp(\Delta V/k_B T)$. If $t_v \gg \tau$ the system falls within the thermal drift regime, with slips both backward and forwards as shown in Fig. 1.5b, and the friction follows the prediction of Krylov et al. [27–29]

$$F \propto \frac{v}{T} e^{1/T}. \quad (1.7)$$

1.4.1.2 Sliding speed

In the thermal activation regime (low temperature) and at low speeds the friction relation follows Eq. (1.6) making friction scale logarithmically with speed. For higher speed, $v > v_c$, if only thermal effects are considered, Eq. (1.6) predicts that friction will eventually saturate and come to a plateau at $F_{\text{fric}} = F_C$. This is illustrated in Fig. 1.6 with this prediction being represented by the dotted line. However, as given away by the figure, for higher speed the model will enter an athermal regime where the thermal effects are negligible compared to other contributions [23](32). In the athermal regime the damping term $m\mu\dot{x}$ will dominate yielding $F_{\text{fric}} \propto v$. The athermal regime is often observed in reduced models if the system is overdamped or at high speeds. This concept is also interesting in connection to MD simulations where the accessible speeds often fall into the athermal regime [30]. It is unclear how this affects real physical systems for which there exist more dissipation channels than just a single viscous term [31]. For the thermal drift regime at higher temperatures the linear relation $F_{\text{fric}} \propto v$ is predicted for low speed as well by Eq. (1.7).

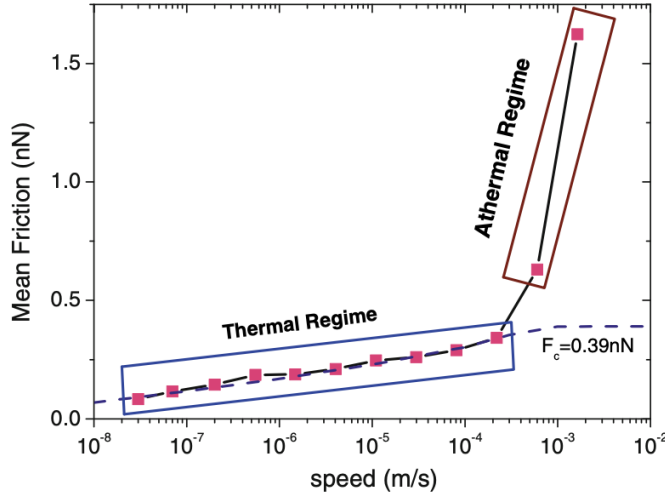


Fig. 6 Speed dependence of friction illustrating two different regimes. In the thermal regime, there is a logarithmic scaling of friction with speed, and in the athermal regime the friction is governed by the damping term such that $F \propto v$. The friction plateau ($F_c = 0.39$ nN) predicted by thermal activation is identified by the dashed line. Other model parameters: $m = 10^{-12}$ kg, $U = 0.6$ eV, $T = 300$ K, $v = 4 \times 10^3$ nm/s, $\mu = 2\sqrt{k/m}$, $a = 0.288$ nm

Figure 1.6: Temporary figure from [23]

1.4.1.3 Tip mass

The mass of the tip affects the dynamics due to a change of inertia, which changes the attempt rate f_0 . Smaller inertia leads to a larger attempt rate and vice versa. Effectively, this will affect the transition point for the temperature and speed regimes described previously. A smaller inertia, giving a larger attempt rate, will cause an earlier transition (i.e. at a lower temperature) to the thermal drift regime, and result in a later speed saturation such that it transitions to the athermal regime at a higher speed.

1.4.1.4 Friction Regimes: Smooth Sliding, Single Slip, and Multiple Slip

Stick-slip motion is a crucial instability mechanism associated with high energy dissipation and high friction. Thus, controlling the transition between smooth sliding and stick-slip is considered key to controlling friction. We can divide the frictional stick-slip behavior into three regimes: 1) Smooth sliding, where the tip slides smoothly on the substrate. 2) Single slip, where the tip sticks at one potential well before jumping one lattice spacing to the next. 3) Multiple slip, where the tip jumps more than one lattice spacing for a slip event. The underlying mechanisms behind these regimes can be understood through static and dynamic contributions.

To understand the static mechanism we consider a quasistatic process for which temperature, speed and damping can be neglected and where we must have $\partial(V)/\partial x = 0$. This simplifies Eq. (1.3) to

$$\frac{\pi U_0}{a} \sin\left(\frac{2\pi x}{a}\right) \frac{2\pi}{a} = K(vt - x). \quad (1.8)$$

The friction regime is determined by the number of solutions x to Eq. (1.8). Only one solution corresponds to smooth sliding, two solutions to a single slip and so on. It turns out that the regimes can be defined by the parameter $\eta = 2\pi^2 U_0 / a^2 K$ [32, 33] yielding transitions at $\eta = 1, 4.6, 7.79, 10.95, \dots$, such that $\eta \leq 1$ corresponds to smooth sliding, $1 < \eta \leq 4.6$ to a single slip and so on. These static derivations lay out the fundamental probabilities for being in one of the regimes stick-slip regimes. Notice that increasing the spring constant K (stiff spring) will decrease the possibilities for stick-slip behavior. This also agrees with Bonelli [Talk about this](#).

Considering the dynamics on top, one finds that damping, speed and temperature will affect this probability. High damping, equivalent to a high transfer of kinetic energy to heat, will result in less energy available for the slip events. This will make multiple slip less likely. By a similar argument, we find that increasing the speed will contribute to more kinetic energy which will increase the likelihood of multiple slips. Finally, the temperature will contribute to earlier slips, due to thermal activation, such that less potential energy can be accumulated and it will result in fewer multiple slips. The effects of damping, speed and temperature are illustrated for the force traces in Fig. 1.7

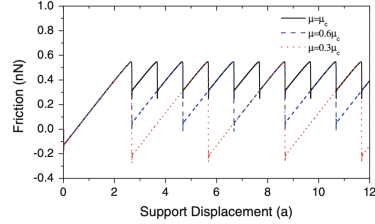


Fig. 9 The effect of damping on transitions between slip regimes where $\mu_c = 2\sqrt{k/m}$ is the critical damping coefficient. Single, double, and triple slip occur at $\mu = \mu_c$, $0.6 \mu_c$, and $0.3 \mu_c$, respectively. The abscissa has units of the lattice spacing a to facilitate identification of the transitions between single, double, and triple regimes. Other model parameters: $U = 0.6 \text{ eV}$, $T = 0 \text{ K}$, $v = 1 \mu\text{m/s}$, $m = 10^{-12} \text{ kg}$, $k = 1 \text{ N/m}$, $a = 0.288 \text{ nm}$

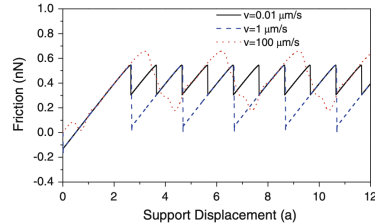


Fig. 10 The effect of sliding speed on transitions between slip regimes. Single, double, and triple slip occur at $v = 100$, 1 , and $0.01 \mu\text{m/s}$, respectively. Other model parameters: $U = 0.6 \text{ eV}$, $T = 0 \text{ K}$, $\mu = 0.8 \mu_c$, $m = 10^{-12} \text{ kg}$, $k = 1 \text{ N/m}$, $a = 0.288 \text{ nm}$

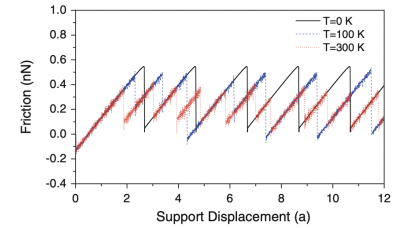


Fig. 11 The effect of temperature on transitions between slip regimes. Other model parameters: $U = 0.6 \text{ eV}$, $v = 1 \mu\text{m/s}$, $\mu = 0.6 \mu_c$, $m = 10^{-12} \text{ kg}$, $k = 1 \text{ N/m}$, $a = 0.288 \text{ nm}$

(a)

(b)

(c)

Figure 1.7: Temporary figure from [23]

1.4.2 Frenkel-Kontorova

The Frenkel-Kontorova (FK) model [34] extends the PT model by considering a chain of atoms in contrast to just a single particle (tip). This extension is useful for understanding the importance of the alignment between the atoms and the substrate, the so-called *commensurability*.

The standard (FK) model consists of a 1D chain of N classical particles of equal mass, representing atoms, interacting via harmonic forces and moving in a sinusoidal potential as sketched in Fig. 1.8 [2]. The Hamiltonian is

$$H = \sum_{i=1}^N \left[\frac{p_i^2}{2m} + \frac{1}{2} K(x_{i+1} - x_i - a_c)^2 + \frac{1}{2} U_0 \cos\left(\frac{2\pi x_i}{a_b}\right) \right], \quad (1.9)$$

where the atoms are labelled sequentially $i = 1, \dots, N$. The first term $p_i^2/2m$ represents the kinetic energy with momentum p_i and mass m . Often the effects of inertia are neglected, referred to as the static FK model, while the inclusion in Eq. (1.9) is known as the dynamic FK model [35]. The next term describes the harmonic interaction with elastic constant K , nearest neighbour distance $\Delta x = x_{i+1} - x_i$ and corresponding nearest neighbour equilibrium distance a_c . The final term represents the periodic corrugation potential, with amplitude U_0 and period a_b . By comparison to the potential used in the PT model Eq. (1.3), the only difference is the introduction of a harmonic coupling between particles in the chain as opposed to the moving body, and that we have not yet specified any force incentivizing sliding. Different boundary choices can be made where both free ends and periodic conditions give similar results. The choice of fixed ends however makes the chain incapable of sliding.

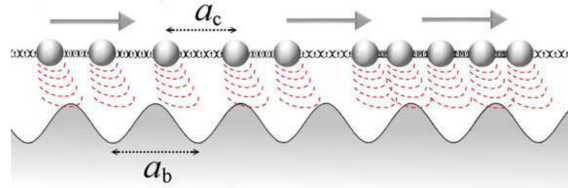


Figure 1. A sketch of the FK model, showing the two competing lengths: the average interparticle spacing and the lattice periodicity of the substrate.

Figure 1.8: [Temporary figure from [2]]

To probe static friction one can apply an external adiabatically increasing force until sliding occurs. This corresponds to the static FK model, and it turns out that the sliding properties are entirely governed by its topological excitations referred to as so-called *kinks* and *antikinks*

1.4.2.1 Commensurability

We can subdivide the frictional behavior in terms of commensurability, that is, how well the spacing of the atoms matches the periodic substrate potential. We describe this by the length ratio $\theta = a_b/a_c = N/M$ where M denotes the number of minima in the potential (within the length of the chain). A rational number for θ means that we can achieve a perfect alignment between the atoms in the chain and the potential minima, without stretching the chain, corresponding to a *commensurate* case. If θ is irrational the chain and substrate cannot fully align without some stretching of the chain, and we denote this as being *incommensurate*.

We begin with the simplest commensurate case of $\theta = 1$ where the spacing of the atoms matches perfectly with the substrate potential periodicity, i.e. $a_c = a_b$, $N = M$. The ground state (GS) is the configuration where each atom is aligned with one of the substrate minima. By adding an extra atom to the chain we would effectively shift some of the atoms, out of this ideal state, giving rise to a kink excitation. This leads to the case where two atoms will have to “share” the same potential corrugation as sketched in Fig. 1.10. On the other hand, removing an atom from the chain results in an antikink excitation where one potential corrugation will be left “atomless”. In order to reach a local minimum the kink (antikink) will expand in space over a finite length such that the chain undertakes a local compression (expansion). Notice that for low ratios of θ , fewer atoms than minima, the chain will not be able to fill each corrugation well in any case, meaning that commensurability can instead be thought of as whether the atoms are forced to deviate, by a lattice spacing, from the spacing otherwise dictated by the spring forces in-between. When applying a tangential force to the chain it is much easier for an excitation to move along the chain than it is for the non-excited atoms since the activation energy ϵ_{PN} for a kink/antikink displacement is systematically smaller (often much smaller) than the potential barrier U_0 . Thus, the motion of kinks (antikinks), i.e. the displacement of extra atoms (atom vacancies), is representing the fundamental mechanism for mass transport. These displacements are responsible for the mobility, diffusivity and conductivity within this model.

In the zero temperature commensurable case with an adiabatical increase in force, all atoms would be put into an accelerating motion as soon as the potential barrier energy is present. However, just as discussed for the PT model, thermal activations will excite the system at an earlier stage resulting in kink-antikink pairs traveling down the chain. For a chain of finite length, these often occur at the end of the chain running in opposite directions. This cascade of kink-antikink excitations is shown in Fig. 1.9. Notice, that for the 2D case, where an island (or flake) is deposited on a surface, we generally also expect the sliding to be initiated by kink-antikink pairs at the boundaries.

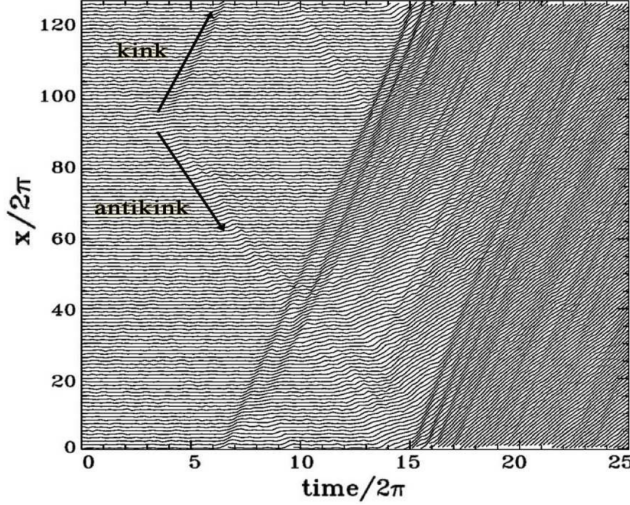


Figure 2. Time dependence of the atomic trajectories for the fully matched ($\theta = 1$) FK model at the (low-temperature) onset of depinning. Motion starts with the nucleation of a kink-antikink pair. The kink and the antikink depart in opposite directions cross the periodic boundary conditions, and collide quasielastically. A second kink-antikink pair forms in the wake of the initial kink. Further kink-antikink pairs are generated, with an avalanche-like increase of the kink-antikink concentration, eventually leading to a sliding state. Adapted from Ref. [21], Copyright (1997) by The American Physical Society.

Figure 1.9: **Temporary** figure from [2]

For the case of incommensurability, i.e. $\theta = a_b/a_c$ is irrational, the GS is characterized by a sort of “staircase” deformation. That is, the chain will exhibit regular periods of regions where the chain is slightly compressed (expanded) to match the substrate potential, separated by kinks (antikinks), where the increased stress is eventually released.



Figure 1.10: **Temporary** figure from [urlhttp://www.iop.kiev.ua/~obraun/myreprints/surveyfk.pdf](http://www.iop.kiev.ua/~obraun/myreprints/surveyfk.pdf) p. 14. Incommensurable case ($\theta = ?$) where atoms sit slightly closer than otherwise dictated by the substrate potential for which this regular result in a kink here seen as the presence of two atoms closely together in one of the potential corrugations.

The incommensurable FK model contains a critical elastic constant K_c , such that for $K > K_c$ the static friction F_s drops to zero, making the chain able to initiate a slide at no energy cost, while the low-velocity kinetic friction is dramatically reduced. This can be explained by the fact that the displacement occurring in the incommensurable case will yield just as many atoms climbing up a corrugation as there are atoms climbing down. For a big (infinite) chain this will exactly balance the forces making it non-resistant to sliding. Generally, incommensurability guarantees that the total energy (at $T = 0$) is independent of the relative position to the potential. However, when sliding freely, a single atom will eventually occupy a maximum of the potential, and thus when increasing the potential magnitude U_0 or softening the chain stiffness, lowering K , the possibility to occupy such a maximum disappears. This marks the so-called Aubry transition, at the critical elastic constant $K = K_c(U_0, \theta)$, where the chain goes from a free sliding to a *pinned* state with nonzero static friction. K_c is a discontinuous function of the ratio θ , due to the reliance on irrational numbers for incommensurability. The minimal value $K_c \simeq 1.0291926$ in units $[2U_0(\pi/a_b)^2]$ is achieved for the golden-mean ratio $\theta = (1 + \sqrt{5}/2)$. Notice

that the pinning is provided despite translational invariance due to the inaccessibility to move past the energy barrier which acts as a dynamical constraint. The Aubry transition can be investigated as a first-order phase transition for which power laws can be defined for the order parameter, but this is beyond the scope of this thesis.

The phenomena of non-pinned configurations are named *superlubricity* in tribological context. Despite the misleading name, this refers to the case where the static friction is zero while the kinetic friction is nonzero but reduced. For the case of a 2D sheet, it is possible to alter the commensurability, not only by changing the lattice spacing through material choice but also by changing the orientation of the sheet relative to the substrate. Dienwiebel et al. [36] have shown that the kinetic friction, for a graphene flake sliding over a graphite surface (multiple layers of graphene), exhibits extremely low friction at certain orientations as shown in Fig. 1.11. Here we clearly see that friction changes as a function of orientation angles with only two spikes of considerable friction force. This relates back to the concept of frictional regimes introduced through the simpler PT model, where the change in orientation affects the effective substrate potential. Merely from the static consideration, we found that lowering the potential amplitude U_0 will decrease the parameter $\eta = 2\pi^2 U_0/a^2 K$ shifting away from the regime of multiple slips towards smooth sliding associated with low friction. Such transitions will also be affected by the shape of the potential and corresponding 2D effects of the sliding path [23].

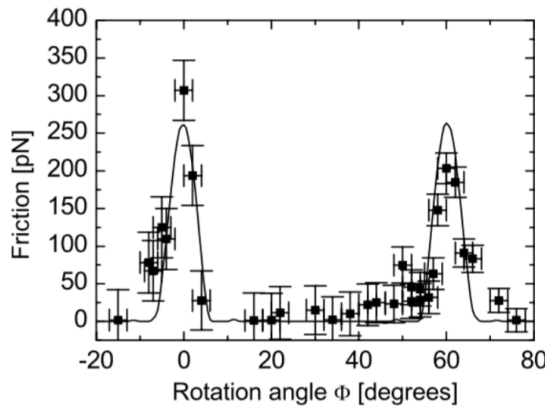


Fig. 6. Average friction force versus rotation angle Φ of the graphite sample around an axis normal to the sample surface. Two narrow peaks of high friction are observed at 0° and 61° , respectively. Between these peaks a wide angular range with ultra-low friction, close the detection limit of the instrument, is found. The first peak has a maximum friction force of 306 ± 40 pN, and the second peak has a maximum of 203 ± 20 pN. The curve through the data points shows results from a Tomlinson model for a symmetric 96-atom graphite flake sliding over the graphite surface (for details about the calculation see [39]).

Figure 1.11: [Temporary] figure from [36] showing superlubricity for incommensurable orientations between graphene and graphite. [temporary]

1.4.2.2 Velocity resonance

While many of the same arguments used for the PT model regarding velocity dependence for friction can be made for the FK model, the addition of multiple atoms introduces the possibility of resonance. In the FK model the kinetic friction is primarily attributed to resonance between the sliding induced vibrations and phonon modes in the chain [35]. The specific dynamics are found to be highly model and dimension specific, and even for the 1D case, this is rather complex. However, we make a simplified analysis of the 1D rigid chain case to showcase the reasoning behind the phenomena.

When all atoms are sliding rigidly with center of mass velocity v_{CM} the atoms will pass the potential maxima with the so-called *washboard frequency* $\Omega = 2\pi v_{CM}/ab$. For a weak coupling between the chain and the potential we can use the zero potential case as an approximation for which the known dispersion relation for the 1D

harmonic chain is given [37, p. 92]

$$\omega_k = \sqrt{\frac{4K}{m}} \left| \sin\left(\frac{k}{2}\right) \right|,$$

where ω_k is the phonon frequency and $k = 2\pi i/N$ the wavenumber with $i \in [N/2, N/2)$. Resonance will occur when the washboard frequency Ω is close to the frequency of the phonon modes ω_q in the chain with wavenumber $q = 2\pi a_c/a_b = 2\pi\theta^{-1}$ or its harmonics nq for $n = 1, 2, 3, \dots$ [38]. Thus, we can approximate the resonance center of mass speed as

$$\begin{aligned} n\Omega &\sim \omega_{nq} \\ n\frac{2\pi v_{CM}}{a_b} &\sim \sqrt{\frac{4K}{m}} \left| \sin\left(\frac{2n\pi\theta^{-1}}{2}\right) \right| \\ v_{CM} &\sim \frac{\sin(n\pi\theta^{-1})}{n\pi} \sqrt{\frac{Ka_b^2}{m}}. \end{aligned}$$

When the chain slides with a velocity around resonance speed, the washboard frequency can excite acoustic phonons which will dissipate to other phonon modes as well. At zero temperature, the energy will transform back and forth between internal degrees of freedom and center of mass movement of the chain. Without any dissipation mechanism this is theorized to speed up the translational decay [35]. However, as soon as we add a dissipation channel through the substrate, energy will dissipate from the chain to the substrate's degrees of freedom. This suggests that certain sliding speeds will exhibit relatively high kinetic friction while others will be subject to relatively low kinetic friction. Simulations of concentric nanotubes in relative motion (telescopic sliding) support this idea as it has revealed the occurrence of certain velocities at which the friction is enhanced, corresponding to the washboard frequency of the system [2], where the friction response was observed to be highly non-linear as the resonance velocities were approached.

The analysis of the phonon dynamics is highly simplified here, and a numerical study of the FK by Norell et al. [35] showed that the behavior was highly dependent on model parameter choices, but that the friction generally increased with velocity and temperature. Here the latter observation differs qualitatively from that of the PT model.

1.4.3 Frenkel-Kontorova-Tomlinson

A final extension of the atomic models worth mentioning here is the Frenkel-Kontorova-Tomlinson (FKT) model [39], which introduces a harmonic coupling of the sliding atom chain to the driving moving body, effectively combining PT and FK (see Fig. 1.3). This introduces more degrees of freedom to the model based on the intention of getting a more realistic connection between the moving body and the chain. modeling of a broad contact point. Dong et al. carried out a numerical analysis using the 1D FKT model investigating the effect of chain length. They observed that the friction increased linearly with the number of atoms in the chain on a long-range, but certain levels of lattice mismatch resulted in local non-linear relationships as shown in Sec. 1.4.3. Similarly, taking the FKT model to 2D they were able to achieve a similar sensitivity to commensurability as observed experimentally by [36] (shown in Fig. 1.11) with the numerical result shown in Sec. 1.4.3. Besides a recreation of the commensurability effect they also observed increasing friction with an increasing flake size. Combined, the 1D and 2D results support the idea of increasing friction with contact size although it might showcase non-linear behavior depending on commensurability.

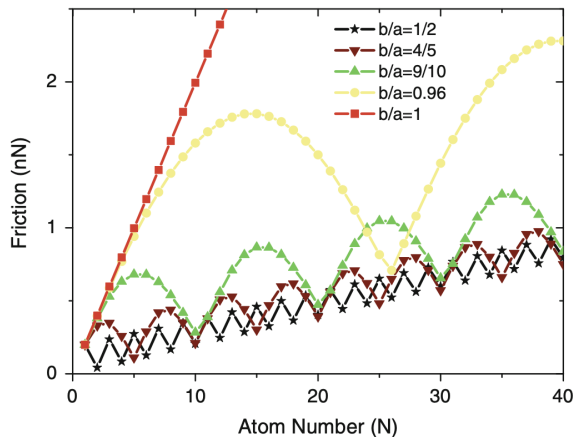


Fig. 21 Friction variation with the tip size N for different lattice mismatch b/a . $k = 5 \text{ N/m}$ and $k_t = 50 \text{ N/m}$ are used to obtain these results

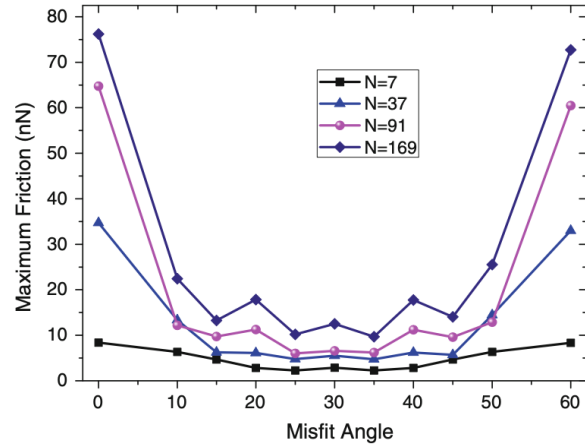


Fig. 23 The misfit angle dependence of friction with different tip sizes; $k_t = 50 \text{ N/m}$ and $k = 10 \text{ N/m}$. The $N = 7$ curve corresponds to the model illustrated in Fig. 22

(a) [Temporary] figure from [23]

(b) [Temporary] figure from [23]

1.4.4 Shortcomings of atomic models

To-DO: Shortcomings of PT-based reduced-models

- Assumes a rigid substrate with a simplified potential shape.
- Energy dissipation is added through a viscous term $-m\mu\dot{x}$ being the only dissipation channel available. Does not capture a more complex real-life electron and phonon dissipation. Taking phonon dissipation as an example there are many vibration modes ($3N$). This will affect the thermal activation derivation.
- The moving body is simplified as a constantly moving rigid body, while in fact this will also be subject to a more complex dynamic behavior.

1.4.5 Experimental procedures

Experimentally, the study of nanoscale friction is challenging due to the low forces on the scale of nano-newtons along with the difficulties of mapping the nano-scale topography of the sample. In opposition to numerical simulations, which provide full transparency regarding atomic-scale structures, sampling of forces, velocities and temperature, the experimental results are limited by the state-of-the-art experimental methods. To compare numerical and experimental results it is useful to address the most common experimental methods.

1.4.5.1 Scanning Probe Microscopy

Scanning probe microscopy (SPM) includes a variety of experimental methods which is used to examine surfaces with atomic resolution [40, pp. 6-27]. This was originally developed for surface topography imaging, but today it plays a crucial role in nanoscale science as it is used for probe-sampling regarding tribological, electronic, magnetic, biological and chemical character. The family of methods involving the measurement of forces is generally referred to as *scanning force microscopies* (SFM) or for friction purposes *friction force microscopes* (FFM).

One such method arose from the *atomic force microscope* AFM, which consists of a sharp micro-fabricated tip attached to a cantilever force sensor, usually with a sensitivity below 1 nN all the way down to pN. The force is measured by recording the bending of the cantilever, either as a change in electrical conduction or more commonly, by a light beam reflected from the back of the cantilever into a photodetector [5, p. 183]. By adjusting the tip-sample height to keep a constant normal force while scanning across the surface, the AFM can be used to produce a surface topography map. By tapping the material (dynamic force microscopy) with

a sinusoidally vibrated tip the effects from friction and other disturbing forces can be minimized to produce an even clearer image (include example, preferably showing the surface structure of graphene). However, when scanning perpendicularly to the cantilever axis, one is also able to measure the frictional force as torsion of the cantilever. By having four quadrants in the photodetector (as shown in figure Fig. 1.13), one can simultaneously measure the normal force and friction force as the probes scan across the surface.

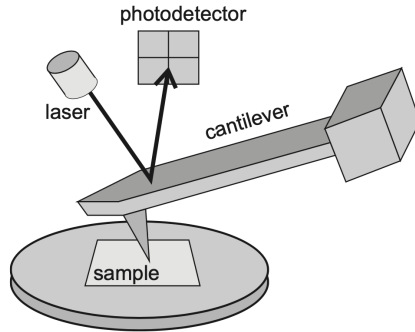


Figure 17.1 Schematic diagram of a beam-deflection atomic force microscope.

Figure 1.13: [Temporary figure from [5, p. 184]

AFM can also be used to drag a nanoflake across the substrate as done by Dienwiebel et al. [36], where a graphene flake was attached to a FFM tip and dragged across graphite. Notice that this makes the normal loading concentrated to a single point on the flake rather than achieving an evenly distributed load.

1.4.5.2 Surface Force Apparatus

The Surface force apparatus SFA is based on two curved molecularly smooth surfaces brought into contact [5, p. 188]. The sample is placed in between the two surfaces as a lubricant film for which the friction properties can be studied by applying a tangential force to the surfaces.

1.5 Summary of previous results

Several studies have investigated the frictional behavior of graphene by varying different parameters such as normal force, sliding velocity, temperature, commensurability and graphene thickness [41]. In general, we find three types of relevant systems being studied: 1) An FFM type setup where the graphene, either resting on a substrate or suspended, is probed by an AFM tip scanning across the surface. 2) A SFA setup with the graphene “sandwiched” in-between two substrate layers moving relative to each other using the graphene as a solid lubricant. 3) A graphene flake sliding on a substrate, either being dragged by an AFM tip or by more complex arrangements in numerical simulations. Considering that even the sharpest AFM tip will effectively put multiple atoms in contact with the sample, all methods are relatable to a nanoscale surface contact. However, the FFM type relates better to asperity theory as we expect it to deform with increasing load, while the latter two are more aligned with the PT type models. We will consider results across all three types of systems with the relevant studies summarized in Table 1.1 for convenience.

Table 1.1: Update multirow line span after completing the table...

System	Type	Year	Researcher	Materials	Keywords
FFM	Exp.	2007 [42]	Zhao et al.	Si ₃ N ₄ tip on graphite.	Temperature dependence
		2015 [43]	G. Paolicelli et al.	Si tip, graphene on SiO ₂ and Ni(111) substrate	Layers, load, shear strength
	Both	2019 [44]	Zhang et al.	Monolayer graphene	Straining sheet
		2019 [45]	Vazirisereshk et al.	Graphene, MoS ₂ and Graphene/MoS ₂ heterostructure	Low friction?
	Num.	2015 [46]	Yoon et al.	Si tip, graphene on SiO ₂	Stick-slip: tip size, scan angle, layer thickness, substrate flexibility
		2016 [47]	Li et al.	Si tip, graphene on a-Si substrate	Increasing layers
	SFA	2011 [48]	Wijn et al.	Graphene flakes between graphite	Rotational dynamics, superlubricity, temperature
		2012 [11]	H. J. Kim and D. E. Kim.	Carbon sheet	Corrugated nano-structured surfaces
Flake	Exp.	2005 [36]	Dienwiebel et al.	Graphene on graphite	Commensurability, superlubricity
		2013 [49]	Feng et al.	Graphene on graphite	Free sliding (relevant?)
	Num.	2009 [50]	Bonelli et al.	Graphene on graphite	Tight-binding, commensurability, load, flake size
		2012 [51]	Reguzzoni et al.	Graphene on graphite	Graphite thickness
		2014 [52]	Liu et al.	Graphene on graphite	Thickness, deformations, high speed
		2018 [53]	P. Zhu and Li	Graphene on gold	Flake size, commensurability
		2019 [54]	Zhang et al.	Graphene on diamond	Temperature, sliding angle, friction coefficient

One of the earliest tribological simulations of graphene was carried out by Bonelli et al. [50] in 2009 using a tight-binding method (excluding thermal excitations) to simulate a graphene flake on an infinite graphene sheet [41]. They implemented a FKT-like setup where each atom in the flake is coupled horizontally to a rigid support by elastic springs. They recovered the stick-slip behavior, which is also observed in FFM setups both experimentally [42, 44] and numerically [47, 53]. Moreover, they found an agreement with the qualitative observation that soft springs allow for a clean stick-slip motion while hard springs ($\sim 40 \text{ N/m}$) inhibit it. In AFM and SFA experiments, the stick-slip motion tend to transition into smooth sliding when the speed exceeds $\sim 1 \mu\text{s}$ while in MD modeling the same transition is observed in the $\sim 1 \text{ m/s}$ region [2]. This 6-order-of-magnitude discrepancy has been largely discussed in connection to simplifying assumptions in MD simulations. On the other hand, the PT model suggest that high speed leads to the multiple slip regime. By considering the force traces predicted by the PT for a high velocity Sec. 1.4.1.4 we notice that the multiple skip might produce a somewhat smoother curve than in the single slip regime. Thus, we might question the definition of smooth sliding when comparing to experimental results which will be derived purely from an force trace curve.

Bonelli et al. [50] also found that commensurability, through orientation of the flake and the direction of sliding, had a great impact on the frictional behavior which generally aligns with the predictions of the FK and FKT models. They confirmed qualitatively the experimental observation of superlubricity for certain incommensurable orientations which is experimentally by Dienwiebel et al. [36] and further supported by experimental measurements of interaction energies by Feng et al. [49]. This commensurability importance is also reported for MD simulations [48, 53, 54]. Bonelli et al. found the friction force and coefficient to be one order of magnitude higher than that of the experimental results which they attribute to the details of the numerical modeling. Generally, the experimental coefficients between graphite and most materials lie in the range 0.08-0.18 [36]. While Dienwiebel et

al. [36] reported a wide range of frictional forces from 28 ± 16 pN to 453 ± 16 pN in a load range $\sim [-10, 20]nN$, the change in friction with applied load was as low as 0.05–0.4 %, yielding a coefficient of 0.0005–0.004 when using the slope definition Eq. (1.2b). This indicates an almost independent relationship between friction and load which they attributes to the lack of change for the contact area.

Furthermore, Bonelli et al. [50] found friction to decrease with increasing flake size which is also reported in MD simulations for graphene on gold [53] in a MD. Bonelli et al. mainly attributes this to boundary effects, but also notes that specifics of the coupling to the support made for decreased rotational freedom as flake size were increased. Thus, they hypothesized that the decreased freedom let to the graphene taking a more force path which can be associated with a decreasing the tendency of stick-slip behavior. The general observation however, disagrees with the FK and FKT model which predicts the reverse, an increase in friction with increasing size.

An additional numerical study of monolayer islands of krypton on copper by Reguzzoni and Righi [55], supports the importance of commensurability in relation to size effects, as they report that the effective commensurability increase drastically below a critical flake radius on the order of 10 Å. In a numerical study by Varini et al. [56], based on Kr islands adsorbed on Pb(111), this is further elaborated as they found that finite size effects are especially important for static friction as a pinning barrier rise from the edge, preventing otherwise superlubricity due to incommensurability. They reported a relationship $F_s \sim A^{\gamma_s}$ not only sublinear $\gamma_s < 1$ but also sublinear to the island perimeter $P \propto A^{1/2}$ by having $\gamma_s = 0.25$ for a hexagonal edge and $\gamma_s = 0.37$ when circular, indicating that only a subset of the edge is responsible for the pinning effect. This aligns with the general change in friction found by [53] for different flake geometries (square, triangle, circle). Additionally, Varini et al. also found the edge pinning effect to decrease with increasing temperature as the edge energy barriers are reduced. Bringing this all together, the main picture forming is that flake size, which can be related to contact area, is affecting friction through a commensurability mechanism. If the flake is constrained in some way we might not observe the same dependency. While flake size nor contact area is easily measured in experimental FFM Mo et al. [8] found that $F_{\text{fric}} \propto A$ where A is the real contact area defined by atoms within chemical range.

Evolution effects, or so-called friction strengthening, are also observed, meaning that the friction force increases during the initial stick-slip cycles. This is observed experimentally by Zhang et al. [44] and numerically by Li et al. [47]. However, this is only found when having the graphene sheet resting on a substrate [44] as opposed to a suspended sheet, and it was found to diminish when increasing number of graphene layers stacked (graphite) [47]. In general, the friction was found to decrease with increasing number of layers which is also supported by the findings in [46] but disagree with [51]?? Zhang et al. [44] additionally found that straining a suspended stretch, modulating the flexibility which consequently change the local pinning capability of the contact interface and lowers the dynamic friction. Another surface manipulating study was performed by H. J. Kim and D. E. Kim. [11] where the investigated the effects of corrugated nano-structured surfaces which altered the contact area and structural stiffness resulting in both increased and slightly decreased friction under certain load ranges. These studies highlight the importance of surface structure and mechanical conditions.

TO-DO: Negative friction coefficients

The dependency on friction of normal load turns out to be a complex matter and has proven to be highly system dependent. As already mentioned, asperity theory mainly point to a sublinear relationship between friction and load, while the PT models points to a dependence through the change of the effective substrate potential leading to a commensurability effect. Experimentally rather different trends have been observed, although the majority agree on an increasing friction with increasing load [5, p. 200]. For the graphene flake Dienwiebel et al. [36] found a seemingly non-dependent relationship while FFM study by G. Paolicelli et al. [43] found a great fit with the sublinear predictions of Maugis-Dugdale theory ($F_f \propto (F_N - F_{N,0})^{2/3}$). Here the discrepancy might lie in the difference between a spherical tip indenting the graphene sheet (matching asperity theory) as opposed to atomic flatness of the graphene/graphite sheets in contact making for a constant contact area. However, numerical studies with graphene in contact with graphite still find both sublinear [50] and linear [54] load dependencies.

The dependency of velocity is generally found to increase logarithmically with velocity in experimental AFM studies [5, p. 201] which match the low velocity regime of the PT type models. At higher velocities thermally activated processes are less important and friction becomes independent of velocity according to the continuation of the Eq. (1.6) without entering the athermal regime related to the PT model which is attributed to a numerical damping effect. The saturation of the velocity dependency has been observed numerically for Si tips and diamond, graphite and amorphous carbon surfaces with scan velocities above $1 \mu\text{s}$ [57]. Guerra et al. [58] studying gold clusters on graphite using MD simulations found a viscous friction response, friction proportional to sliding

velocity, in both low and high speed domains. However, thermal effects reversed: at low speed (diffusive) friction decreased with increased temperature while at high speed (ballistic) speed friction increases with temperature. In the MD simulations the crossover from ballistic to diffusive occurred between 10 and 1 m/s.

For the temperature the general experimental trend is an decreasing friction with increasing temperature as found by Zhao et al. [42] in a series of AFM graphene on graphite experiments with $F_{\text{fric}} \propto \exp(1/T)$. This agrees with the thermal drift regime of the PT type models even though the temperature range used in the study does not match the range of this regime according to the PT model. Wijn et al. [48] find that friction commensurability can be lost at higher temperature (above 200K) were the found a power law behavior $F_k \propto T^{-1.13 \pm 0.04}$. Numerically, Zhang et al. [54] found that friction increased with temperature, using a velocity of 10 m/s. Considering the findings of [58] related to MD this qualitative different dependence might be due the to low speed diffisive behaviour as opposed to high speed ballistic behavior in MD simulations.

A summary of the expectations is given in Table 1.2.

1.6 Research questions

Table 1.2: Summary

Stick slip	Generally we expect to observe periodic stick-slip motion with a period matching the lattice constant(s) involved [8]. This is however expected to be inhibited by high spring stiffness for the moving support. At large velocities the reduced-models suggest a multiple slip behavior while experimental results suggest smooth sliding. This discrepancy might be explained by a different definition of smooth sliding as the multiple slip regime can produce seemingly “smooth-looking” force traces. Additionally, it is expected that the tendency of stick-slip behaviour is reduced by increasing temperature and for incommensurability.
Static friction	The static friction is highly related to the presence of stick-slip motion. The static friction is most pronounced for commensurable configurations and will decrease drastically for incommensurability. However, further reduction of static friction is expected for an increasing flake size and increasing temperature.
Commensurability	Both static and dynamic friction is expected to be highly sensitive to commensurability, through lattice spacing, orientation of the flake relative to the substrate and by the path of sliding along the substrate. By changing the spring stiffness of the coupled driving support we expect to get a response in commensurability due to a change in translational freedom.
Friction evolution (Friction strengthening)	Friction evolution is found to be present in mono layer graphene resting on a substrate, and thus we expect this to be present in our simulation setup as well.
Negative coef	TO-DO
Normal load	Generally an increasing friction force is expected with increasing load. Both non-dependent, sublinear and linear relationship can be expected here.
Velocity	Generally an increasing friction force is expected with increased sliding velocity. Experimental results suggest that kinetic friction goes as $F_k \propto \ln(v)$, with the expectation that friction becomes independent of velocity at “high” velocities above $1 \mu\text{m/s}$. Numerically a viscous $F_k \propto v$ is expected for all velocity ranges.
Temperature	Experimentally and numerically friction is expected to decrease with friction in a power law or exponential manner. However, for high velocity ranges, according to a ballistic regime, which might coincide with the capabilities of MD, the friction is predicted to increase with temperature.
Contact area	For our system we do not expect any contact area changes during load, however an increasing number of atoms in contact is expected to increase friction.

Part II

Simulations

Appendices

Appendix A

Appendix B

Appendix C

Bibliography

- ¹H.-J. Kim and D.-E. Kim, “Nano-scale friction: a review”, *International Journal of Precision Engineering and Manufacturing* **10**, 141–151 (2009).
- ²N Manini, O. M. Braun, E Tosatti, R Guerra, and A Vanossi, “Friction and nonlinear dynamics”, *Journal of Physics: Condensed Matter* **28**, 293001 (2016).
- ³Bhusnur, “Introduction”, in *Introduction to tribology* (John Wiley & Sons, Ltd, 2013) Chap. 1, 1–?
- ⁴B. Bhushan and A. V. Kulkarni, “Effect of normal load on microscale friction measurements”, *Thin Solid Films* **278**, 49–56 (1996).
- ⁵E. Gnecco and E. Meyer, *Elements of friction theory and nanotribology* (Cambridge University Press, 2015).
- ⁶J. Gao, W. D. Luedtke, D. Gourdon, M. Ruths, J. N. Israelachvili, and U. Landman, “Frictional forces and amontons’ law: from the molecular to the macroscopic scale”, *The Journal of Physical Chemistry B* **108**, Publisher: American Chemical Society, 3410–3425 (2004).
- ⁷J. H. Dieterich, “Time-dependent friction in rocks”, *Journal of Geophysical Research (1896-1977)* **77**, 3690–3697 (1972).
- ⁸Y. Mo, K. T. Turner, and I. Szlufarska, “Friction laws at the nanoscale”, *Nature* **457**, 1116–1119 (2009).
- ⁹G. Carbone and F. Bottiglione, “Asperity contact theories: do they predict linearity between contact area and load?”, *Journal of the Mechanics and Physics of Solids* **56**, 2555–2572 (2008).
- ¹⁰F. Bowden and D. Tabor, *The friction and lubrication of solids*, International series of monographs on physics vb. 1 (Clarendon Press, 2001).
- ¹¹H.-J. Kim and D.-E. Kim, “Molecular dynamics simulation of atomic-scale frictional behavior of corrugated nano-structured surfaces”, *Nanoscale* **4**, 3937–3944 (2012).
- ¹²W. Commons, *File:asperities.svg — wikimedia commons, the free media repository*, [Online; accessed 3-February-2023], 2022.
- ¹³I. Szlufarska, M. Chandross, and R. W. Carpick, “Recent advances in single-asperity nanotribology”, *Journal of Physics D: Applied Physics* **41**, 123001 (2008).
- ¹⁴G. Binnig, C. F. Quate, and C. Gerber, “Atomic force microscope”, *Phys. Rev. Lett.* **56**, 930–933 (1986).
- ¹⁵S. S. Perry, “Scanning Probe Microscopy Measurements of Friction”, *MRS Bulletin* **29**, 478–483 (2004).
- ¹⁶Hertz, “On the contact of elastic solids”, *Crelle’s Journal* **92**, 156–171.
- ¹⁷D. Maugis, “Adhesion of spheres: the jkr-dmt transition using a dugdale model”, *Journal of Colloid and Interface Science* **150**, 243–269 (1992).
- ¹⁸M. H. Müser, “Rigorous field-theoretical approach to the contact mechanics of rough elastic solids”, *Phys. Rev. Lett.* **100**, 055504 (2008).
- ¹⁹B. N. J. Persson, “Theory of rubber friction and contact mechanics”, *The Journal of Chemical Physics* **115**, 3840–3861 (2001).
- ²⁰J. A. Greenwood and J. B. P. Williamson, *Contact of nominally flat surfaces*, en, 1966.
- ²¹A. Bush, R. Gibson, and T. Thomas, “The elastic contact of a rough surface”, *Wear* **35**, 87–111 (1975).
- ²²B. Luan and M. O. Robbins, “The breakdown of continuum models for mechanical contacts”, *Nature* **435**, 929–932 (2005).

- ²³Y. Dong, A. Vadakkepatt, and A. Martini, “Analytical models for atomic friction”, *Tribology Letters* **44**, 10.1007/s11249-011-9850-2 (2011).
- ²⁴E. Gnecco, R. Bennewitz, T. Gyalog, C. Loppacher, M. Bammerlin, E. Meyer, and H.-J. Güntherodt, “Velocity dependence of atomic friction”, *Phys. Rev. Lett.* **84**, 1172–1175 (2000).
- ²⁵P. Hänggi, P. Talkner, and M. Borkovec, “Reaction-rate theory: fifty years after kramers”, *Rev. Mod. Phys.* **62**, 251–341 (1990).
- ²⁶Y. Sang, M. Dubé, and M. Grant, “Thermal effects on atomic friction”, *Phys. Rev. Lett.* **87**, 174301 (2001).
- ²⁷S. Y. Krylov, K. B. Jinesh, H. Valk, M. Dienwiebel, and J. W. M. Frenken, “Thermally induced suppression of friction at the atomic scale”, *Phys. Rev. E* **71**, 065101 (2005).
- ²⁸S. Krylov and J. Frenken, “Thermal contact delocalization in atomic scale friction: a multitude of friction regimes”, English, *New Journal of Physics* **9**, 10.1088/1367-2630/9/10/398 (2007).
- ²⁹K. B. Jinesh, S. Y. Krylov, H. Valk, M. Dienwiebel, and J. W. M. Frenken, “Thermolubricity in atomic-scale friction”, *Phys. Rev. B* **78**, 155440 (2008).
- ³⁰Q. Li, Y. Dong, D. Perez, A. Martini, and R. W. Carpick, “Speed dependence of atomic stick-slip friction in optimally matched experiments and molecular dynamics simulations”, *Phys. Rev. Lett.* **106**, 126101 (2011).
- ³¹Y. Dong, Q. Li, and A. Martini, “Molecular dynamics simulation of atomic friction: a review and guide”, *Journal of Vacuum Science & Technology A* **31**, 030801 (2013).
- ³²K. Johnson and J. Woodhouse, “Stick-slip motion in the atomic force microscope”, *Tribology Letters* **5**, 155–160 (1998).
- ³³S. N. Medyanik, W. K. Liu, I.-H. Sung, and R. W. Carpick, “Predictions and observations of multiple slip modes in atomic-scale friction”, *Phys. Rev. Lett.* **97**, 136106 (2006).
- ³⁴J. Frenkel and T. Kontorova, “On the theory of plastic deformation and twinning”, *Phys. Z. Soviet.* **13** (1938).
- ³⁵J. Norell, A. Fasolino, and A. Wijn, “Emergent friction in two-dimensional frenkel-kontorova models”, *Physical Review E* **94**, 10.1103/PhysRevE.94.023001 (2016).
- ³⁶M. Dienwiebel, N. Pradeep, G. S. Verhoeven, H. W. Zandbergen, and J. W. Frenken, “Model experiments of superlubricity of graphite”, *Surface Science* **576**, 197–211 (2005).
- ³⁷C. Kittel, *Introduction to solid state physics*, 8th ed. (Wiley, 2004).
- ³⁸J. A. van den Ende, A. S. de Wijn, and A. Fasolino, “The effect of temperature and velocity on superlubricity”, *Journal of Physics: Condensed Matter* **24**, 445009 (2012).
- ³⁹M. Weiss and F.-J. Elmer, “Dry friction in the Frenkel-Kontorova-Tomlinson model: dynamical properties”, *Zeitschrift für Physik B Condensed Matter* **104**, 55–69 (1997).
- ⁴⁰B. Bhushan, “Nanotribology and nanomechanics”, *Wear* **259**, 15th International Conference on Wear of Materials, 1–? (2005).
- ⁴¹O. Penkov, H.-J. Kim, H.-J. Kim, and D.-E. Kim, “Tribology of graphene: A review”, *International Journal of Precision Engineering and Manufacturing* **15**, 577–585 (2014).
- ⁴²X. Zhao, M. Hamilton, W. G. Sawyer, and S. S. Perry, “Thermally activated friction”, *Tribology Letters* **27**, 113–117 (2007).
- ⁴³G Paolicelli, M Tripathi, V Corradini, A Candini, and S Valeri, “Nanoscale frictional behavior of graphene on sio₂ and ni(111) substrates”, *Nanotechnology* **26**, 055703 (2015).
- ⁴⁴S. Zhang, Y. Hou, S. Li, L. Liu, Z. Zhang, X.-Q. Feng, and Q. Li, “Tuning friction to a superlubric state via in-plane straining”, *Proceedings of the National Academy of Sciences* **116**, Publisher: Proceedings of the National Academy of Sciences, 24452–24456 (2019).
- ⁴⁵M. R. Vazirisereshk, H. Ye, Z. Ye, A. Otero-de-la Roza, M.-Q. Zhao, Z. Gao, A. T. C. Johnson, E. R. Johnson, R. W. Carpick, and A. Martini, “Origin of nanoscale friction contrast between supported graphene, mos₂, and a graphene/mos₂ heterostructure”, *Nano Letters* **19**, PMID: 31267757, 5496–5505 (2019).
- ⁴⁶H. M. Yoon, Y. Jung, S. C. Jun, S. Kondaraju, and J. S. Lee, “Molecular dynamics simulations of nanoscale and sub-nanoscale friction behavior between graphene and a silicon tip: analysis of tip apex motion.”, *Nanoscale* **7** 14, 6295–303 (2015).

- ⁴⁷S. Li, Q. Li, R. W. Carpick, P. Gumbsch, X. Z. Liu, X. Ding, J. Sun, and J. Li, “The evolving quality of frictional contact with graphene”, *Nature* **539**, Number: 7630, 541–545 (2016).
- ⁴⁸A. Wijn, A. Fasolino, A. Filippov, and M. Urbakh, “Low friction and rotational dynamics of crystalline flakes in solid lubrication”, *Europhysics Letters (epl)* **95**, 10.1209/0295-5075/95/66002 (2011).
- ⁴⁹X. Feng, S. Kwon, J. Y. Park, and M. Salmeron, “Superlubric sliding of graphene nanoflakes on graphene”, *ACS Nano* **7**, Publisher: American Chemical Society, 1718–1724 (2013).
- ⁵⁰F. Bonelli, N. Manini, E. Cadelano, and L. Colombo, “Atomistic simulations of the sliding friction of graphene flakes”, *The European Physical Journal B* **70**, 449–459 (2009).
- ⁵¹M. Reguzzoni, A. Fasolino, E. Molinari, and M. C. Righi, “Friction by shear deformations in multilayer graphene”, *The Journal of Physical Chemistry C* **116**, 21104–21108 (2012).
- ⁵²Y. Liu, F. Grey, and Q. Zheng, “The high-speed sliding friction of graphene and novel routes to persistent superlubricity”, *Scientific Reports* **4**, 4875 (2014).
- ⁵³P. Zhu and R. Li, “Study of nanoscale friction behaviors of graphene on gold substrates using molecular dynamics”, *Nanoscale Research Letters* **13**, 34 (2018).
- ⁵⁴J. Zhang, E. Osloub, F. Siddiqui, W. Zhang, T. Ragab, and C. Basaran, “Anisotropy of graphene nanoflake–diamond interface frictional properties”, *Materials* **12**, 10.3390/ma12091425 (2019).
- ⁵⁵M. Reguzzoni and M. C. Righi, “Size dependence of static friction between solid clusters and substrates”, *Phys. Rev. B* **85**, 201412 (2012).
- ⁵⁶N. Varini, A. Vanossi, R. Guerra, D. Mandelli, R. Capozza, and E. Tosatti, “Static friction scaling of physisorbed islands: the key is in the edge”, *Nanoscale* **7**, 2093–2101 (2015).
- ⁵⁷O Zwörner, H Hölscher, U. Schwarz, and R Wiesendanger, “The velocity dependence of frictional forces in point-contact friction”, *APPLIED PHYSICS A MATERIALS SCIENCE AND PROCESSING* **66**, S263–S268 (1998).
- ⁵⁸R. Guerra, U. Tartaglino, A. Vanossi, and E. Tosatti, “Ballistic nanofriction”, *Nature Materials* **9**, 634–637 (2010).